JMEPEG (2007) 16:655–662
DOI: 10.1007/s11665-007-9084-5

1059-9495/$19.00

Metallurgical Evaluation of AZ31B-H24 Magnesium Alloy Friction Stir Welds

M. Pareek, A. Polar, F. Rumiche, and J.E. Indacochea

(Submitted August 10, 2006; in revised form September 11, 2006)

Friction Stir welding of 3.175 mm (0.125 in.) thick plates of AZ31-H24 magnesium alloy was performed using several travel velocities and tool-rotation speeds. After production the welds were cross-sectioned and a metallurgical characterization was performed using optical microscopy, and scanning electron microscopy. Assessment of the weld nugget or "stirred zone" shows evidence of dynamic recrystallization and the start of grain growth in some spots of this region compared to the parent metal. Recrystallization was identified in the thermomechanically affected zone (TAZ) as well. The mechanical properties of the weld are correlated with the corresponding microstructures present in the weld nugget and TMAZ. Corrosion resistance of the weld was assessed using Electrochemical Impedance Spectroscopy (EIS) techniques and immersion tests in a corrosive environment; it showed better corrosion resistance than the base metal.

Keywords Automotive, Joining, Metallography

1. Introduction

The demands of weight reduction in the automobile industry in the context of fuel savings, metal recyclability and emission reduction has prompted focus on lightweight metals such as aluminum and magnesium. Conventional fusion welding methods of joining of magnesium alloys frequently result in defects such as porosity and hot crack, which decline the mechanical properties. Friction stir welding (FSW) has the potential to provide defect free welds in materials of poor fusion weldabiltiy. FSW is a solid-state joining technique developed at the Welding Institute (TWI) in Cambridge (Ref 1). In this process a rotating tool with a profiled pin is plunged along the joint line. As it traverses along the joint the frictional heat generated, plasticizes the material. The tool pin then forges and extrudes the two pieces together by heat and force. It provides a constant hot-working action that transports the plasticized material from the leading face of the tool to the trailing edge, where consolidation produces a continuous joint.

Conservation of nonrenewable resources has become extremely important in recent times. The challenges of significant weight reduction in the automobile and aerospace industry in context of significant fuel savings, recyclability, and emission reduction have promoted focus on lightweight metals such as aluminum and magnesium. Correspondingly, new approaches and processes for joining extrusions and castings in body frames and automotive body panels have been pursued. To date, magnesium's growth rate in the automotive market in North America and Europe has exceeded 20% per year over the period from 1993 to 1997 and continues to rise. Magnesium offers lower density and has highest strength to weight ratio of all structural metals. Also, magnesium is abundant and is the eighth most common element and is recyclable. Magnesium has the potential to replace polymers due to its high mechanical properties, high damping capacity, and electromagnetic shielding which are lacking in polymers (Ref 2).

Conventional fusion welding methods for joining magnesium alloys produce some defects such as porosity and hot crack, which deteriorate their mechanical properties. The production of the defect free weld requires complete elimination of the surface oxide layer and selection of suitable welding parameters. Magnesium alloys are currently welded using techniques such as gas tungsten arc welding (GTAW) and gas metal arc welding (GMAW); while reasonable welding speeds can be achieved, problems can be experienced such as high-welding-residual stresses and changes in microstructure resulting from melting and solidification. High-purity-shielding gases are necessary to prevent weld contamination; magnesium alloys can readily oxidize in the weld zone because of their high-chemical reactivity at high temperatures.

Friction Stir Welding provides defect free welds in materials with poor fusion weldability. This process can also accomplish important cost savings due to elimination of weld defects, filler materials, shielding gases, and weld preparation compared to fusion welding. In the present investigation the focus is on AZ31B-H24 magnesium alloy, which has applications as aircraft fuselage (Ref 3), automobile constructional parts, components, and machine tool parts undergoing rapid acceleration and retardation (Ref 4). Our objective is to investigate the microstructural changes due to friction stir welding of a magnesium alloy AZ31B-H24 alloy and analyze their effect on mechanical properties and corrosion behavior of the alloy.

M. Pareek, A. Polar, F. Rumiche, and **J.E. Indacochea,** Materials Engineering, Joining Science and Advanced Materials Research Laboratory, University of Illinois at Chicago, Chicago, IL. Contact e-mail: jeindaco@uic.edu.

2. Experimental Work

The as-received AZ31B-H24 magnesium alloy was strain hardened and partially annealed, its chemical composition in wt. %, was Al: 2.5-3.5; Zn: 0.6-1.4; Mn: 0.2-1.0; Si: 0.1 max; Fe: 0.005 max; Cu: 0.04 max; Ni: 0.005 max; other: 0.3 max; and Mg: balance. Coupons 3.175 mm (0.125 in.) thick were welded using two tool rotational speeds of 1500 and 2000 rpm at travel speeds of 1.3, 2.1, and 3.4 mm/s (3, 5, and 8 in./min). The FSW rotating tool was made of D2 steel. The friction stir welds were fabricated using a CNC machine. The welds were cross-sectioned, prepared metallographically, and analyzed using a LECO 300 Metallograph. Tensile tests were carried out in an Instron tensile machine at the strain rate of 0.42 mm/s (1 in /min). The fractured surfaces of the tensile specimens were examined in a HITACHI 3000 Scanning Electron Microscope that has an energy dispersive spectrometer (EDS) attachment.

The corrosion behavior of the AZ31B-H24 FS welds, the as-received plate, and annealed alloy was studied by means of potentiodynamic tests, electrochemical impedance spectroscopy, and immersion corrosion tests. All tests were performed in aerated corrosive water solution at room temperature according to ASTM D-1384 (pH = 8.4). This media was chosen because the sulfate, chloride, and bicarbonate ions present simulate the ions present in the atmosphere. Also chlorides and sulfates hold moisture on the surface that can promote corrosion. Presence of chloride is a major factor of concern to most magnesium alloy users.

3. Results and Discussion

3.1 Microstructural Features

The microstructure of the as-received Mg-alloy was fine grained with a mean grain diameter of 5.5 μm, as seen in Fig. 1. The friction stir welds were defect free and had no cavities. Onion ring structures were observed in these magnesium alloy welds similar to what we had found when friction stir welding aluminum. The emergence of the onion ring structure can be attributed to a geometrical effect of the tool, instigated by rotation of the tool and its forward movement. The tool pin grabs the plasticized metal in front of the tool, extrudes it around to the retreating side of the weld and deposits it behind the weld tool. The onion ring structure has been found to have no effect on the mechanical properties of the weld. Another notable microstructural feature of these welds was the segregation of dispersoids to the advancing side of the weld (Fig. 2), and only few dispersoids were found at the retreating side, as seen in Fig. 3. Volume fraction measurements and microchemical EDS analysis of the dispersoids were performed; this evaluation was done at each side of the weld with the sample in the as-polished condition. This information is reported in Table 1; the EDS analysis of the particles shows that the small ones are just magnesium oxide (97.7 wt. % Mg and 2.3 wt. % O), while the larger particles contained Mn and Al in addition to Mg and O (68.3 wt.% Mg, 20.5 wt.% Mn, 9.0 wt.% Al, and 2.2 wt.% O). It is believed that the oxides at the advancing side may be the result of preexisting oxides or might have formed by the oxidation of Mg and alloying elements during friction stir welding. The segregation of these oxides to the advancing side is caused by the material flow owed to the rotating tool in conjunction with the direct

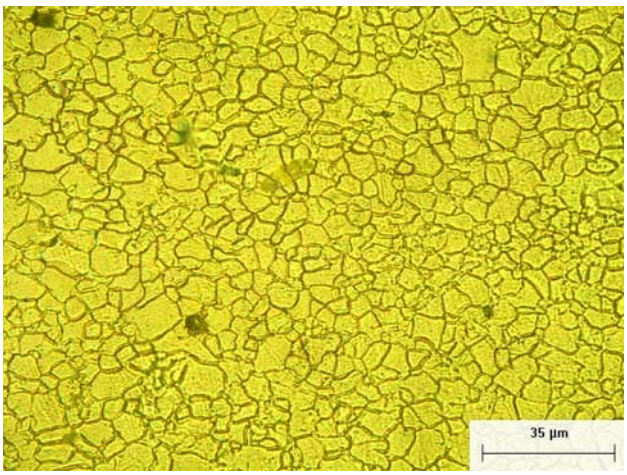

Fig. 1 Photomicrograph of the as-received magnesium alloy normal to the rolling direction

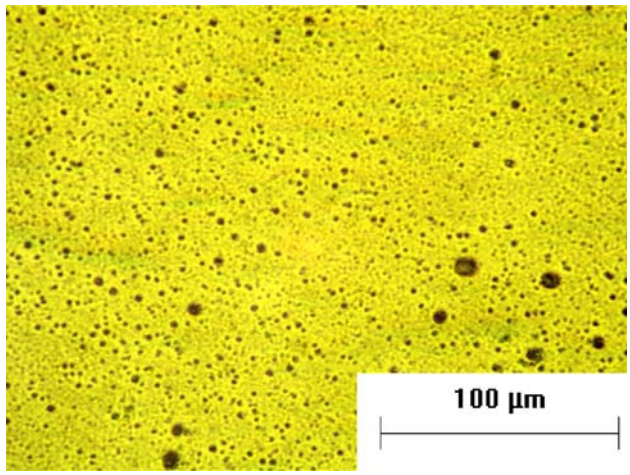

Fig. 2 Dispersoids found in the advancing side of the weld

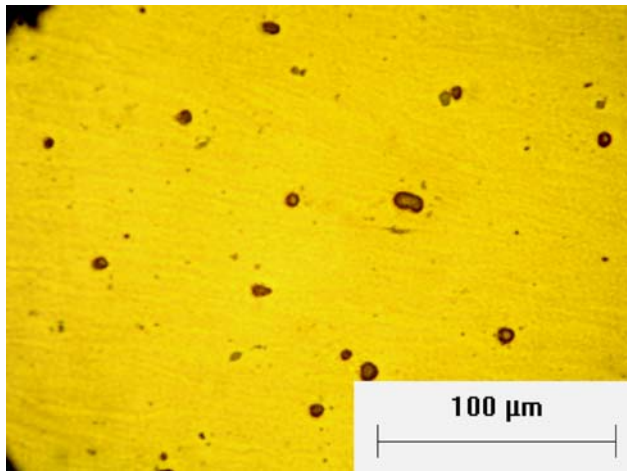

Fig. 3 Dispersoid concentration at the retreating side of the weld

extrusion of the shoulder and the stirring action of the tool pin (Ref 5). As the material is extruded from the retreating side to the advancing side, the stirring and forging action of the tool breaks the oxide particles, which collectively flow and entrain into the nugget zone.

3.1.1 Deformation and Annealing Processes during FSW. It is known that the weld metal experiences excessive strains, high strain rates, and high temperatures (≥0.5 T_m of the base metal) during friction stir welding. The total free energy of a crystalline material is raised during deformation by the presence of dislocations and interfaces; thus, a material with these defects is thermodynamically unstable. The stacking fault energy (SFE), which is unique to each material, determines the extent to which unit dislocations dissociate into partial dislocations. Low SFE promotes dissociation of dislocations and hinders their climb and cross slip which are basic mechanisms responsible for recovery. Mg has low SFE, about 60-78 mJ/m^2 (Ref 6).

Tan et al. (Ref 7) attributed the dynamic recrystallization during the hot deformation of Mg-3Al-1Zn to the constraints imposed by the lack of easily activated slip systems in HCP-Mg. They explained that dynamic recrystallization of this alloy can also be attributed to the higher-angle grain boundary diffusion rate of Mg than Al, and by dislocations being absorbed by the grain boundaries. Dynamic recrystallization during friction stir welding was reported by Esperaza et al., as well (Ref 8). It is suspected that during friction stir welding of AZ31B-H24, in our study, a large strain is introduced by the tool pin and high temperatures develop from friction during FSW; both factors combine to produce dynamic recrystallization and grain growth in the weld. In order to evaluate the microstructure evolution of the different friction stir welds produced in this study, key locations of the weld cross-section were selected, as illustrated in Fig. 4.

Table 1 Volume fraction of dispersoids

	% Volume Fraction	
Parameter	**Advancing side**	**Retreating side**
1500 rpm—1.3 mm/s (3 ipm)	1.91	0.60
1500 rpm—2.1 mm/s (5 ipm)	1.68	0.51
1500 rpm—3.4 mm/s (8 ipm)	2.57	1.03
2000 rpm—1.3 mm/s (3 ipm)	1.55	0.56
2000 rpm—2.1 mm/s (5 ipm)	2.51	0.59
2000 rpm—3.4 mm/s (8 ipm)	2.53	1.04

Since the as-received material was strain hardened and partially annealed, the base plate was submitted to annealing to find out the impact of the remaining strain on the recrystallization and grain growth of the base metal microstructure. The annealing was undertaken for about 30 min at about 350 °C; this temperature was related to the peak temperature of the weld nugget, which was indirectly recorded near the FS weld. As a result of annealing the base metal experienced grain coarsening (~8.8 μm).

3.1.2 Grain Structure in the Weld. The mean grain size across all weld samples was coarser than the mean grain size of the as-received (5.3 μm) and annealed (8.8 μm) Mg alloy samples. Figures 5 and 6 display the grain microstructure at the center of the weld nugget, (position B in Fig. 4), for the welds produced at 1500 rpm—1.3 mm/s (3 ipm) and 2000 rpm—3.4 mm/s (8 ipm) respectively; grain sizes of 12.8 μm and 12.0 μm were measured. Grain size measurements were performed for the two other travel speeds and plotted in Fig. 7. It is observed that regardless of the tool rpm and travel speed, all welds underwent grain coarsening compared to the as-received and annealed microstructures. Grain size measurements were conducted at three selected spots of the weld metal identified in Fig. 4, (A, B, and C) to assess the effect of process parameters on grain size. The bottom portion of the weld had the coarsest-grain diameter, followed by the weld center; the top portion of the weld had the smallest grains. It seems that for a fixed rotation speed, the increase in tool travel speed leads to a reduction in mean grain diameter, as seen in Fig. 7. In contrast, there was a slight increase in grain diameter as the rotation speed changed from 1500 rpm to 2000 rpm for each travel speed. The fact that the mean grain diameter of all welds was coarser than both the as-received and annealed samples suggests that all weld microstructures underwent dynamic recrystallization and grain growth.

The decrease in grain diameter with travel speed could be attributed to the greater straining of the metal derived from the process parameters, which activates more strain free nucleation sites. As the nucleation rate increases, the grain growth becomes more competitive, resulting in a finer-mean grain diameter. The increase in grain size as the tool rotation increases from 1500 rpm to 2000 rpm has to be caused by the higher-temperatures expected at the faster-rotation speed.

The critical temperature for dynamic recrystallization is related to the deformation temperature (T), the total strain (ε) and the strain rate ($\dot{\varepsilon}$). The Zener-Hollomon parameter (Z) equation (Ref 9) incorporates all these variables:

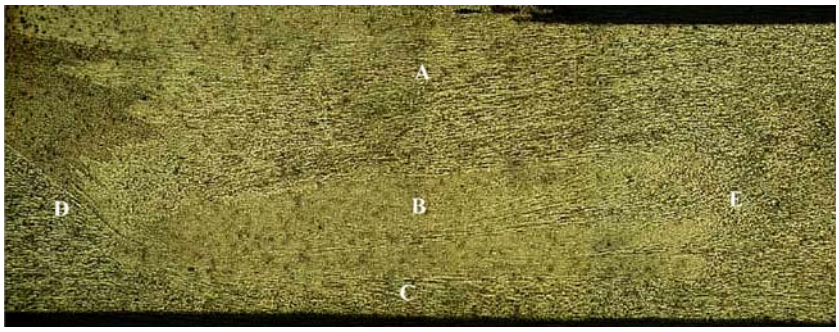

Fig. 4 FSW produced at 1500 rpm and 1.3 mm/s (3 ipm). This weld is used to analyze the microstructure development at different spots: (A) weld nugget top; (B) center of weld nugget; (C) bottom of the weld nugget; (D) TMAZ at the advancing side; and (E) TMAZ at the retreating side

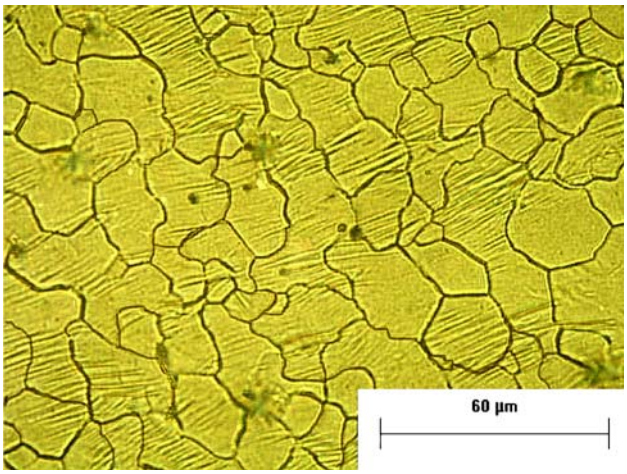

Fig. 5 Grain microstructure from the center of the weld. FSW produced at 1500 rpm and 1.3 mm/s (3 ipm)

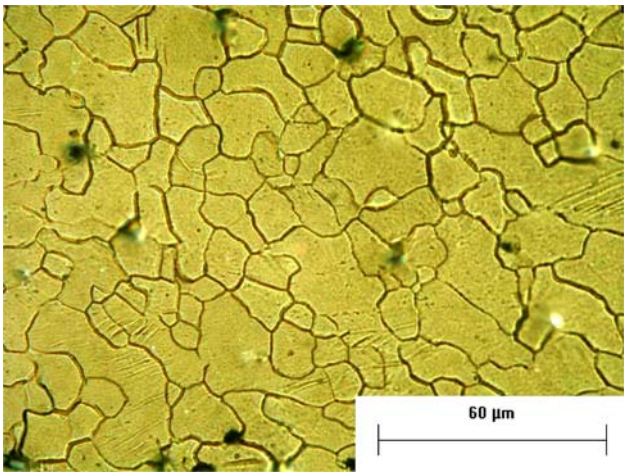

Fig. 6 Grain microstructure from the center of the weld. FSW produced at 2000 rpm and 3.4 mm/s (8 ipm)

$$Z = \dot{\varepsilon} \cdot e^{\frac{Q}{RT}} \quad \text{(Eq 1)}$$

where, Q is activation energy, which is 135 kJ/mol for lattice diffusion in Mg; R is the gas constant; and T is the absolute temperature. Chang et al. (Ref 10) established a relationship between grain size and Z for friction stir processed (FSP) Mg alloy AZ31B alloy specified by the empirical equation:

$$\ln d = 9.0 - 0.27 \cdot \ln Z \quad \text{(Eq 2)}$$

where, d is the dynamically recrystallized grain size. Barnett et al. (Ref 11), on the other hand, established a relationship between dynamically recrystallized grain size, d_{DRX}, and Z for AZ31B alloy tested in tension as

$$d_{DRX} = 77 \cdot Z^{-0.1} \quad \text{(Eq 3)}$$

Both studies showed that the average recrystallized grain size would be refined with decreasing working temperature and increasing strain rate. In this study as the weld travel speed is adjusted from 1.3 mm/s (3 ipm) to 3.4 mm/s (8 ipm) the strain rate increases; but then, as the rotation speed raises from 1500 to 2000 rpm the frictional heat generated would be greater. Therefore, the grain size in the dynamically recrystallized weld nugget is expected to be reduced as the travel speed is increased, and the tool rotational speed is maintained constant; on the other hand the dynamic recrystallized grain size becomes coarser with increase in the rotation speed for a constant weld travel speed.

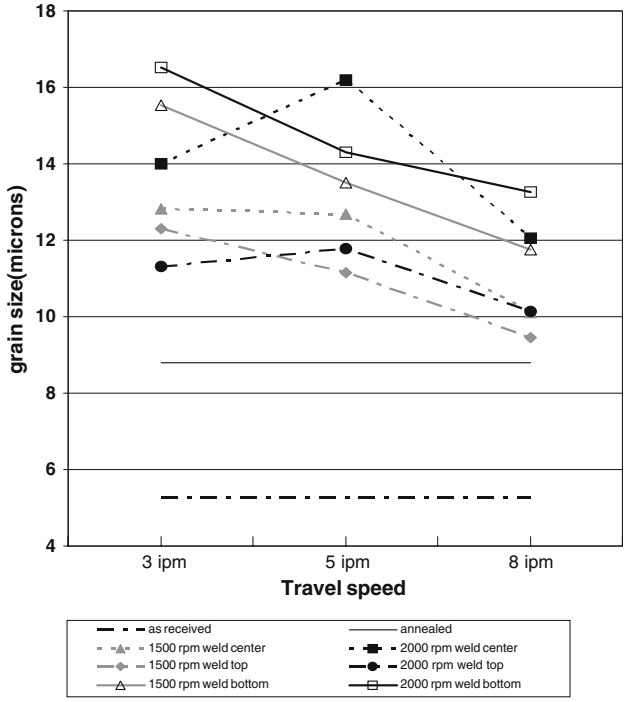

Fig. 7 Grain size measurements in the weld

The grain size at the top of the weld is the finest compared to the center and bottom regions of the weld nugget (Fig. 7). The shoulder forges the material at the top of the weld introducing severe strains that contribute to the very fine grain structure. The grains at this location became finer as the travel speed increased, but it was observed that the increase in the rotation speed did not have any effect; it is likely that the proximity of this region to the surface allow for a faster cooling which reduced the dwell time of this region above the critical temperature for significant grain growth.

3.1.3 Grain Structure and Dimensions in the TMAZ. Alike the weld nugget, the average grain sizes at both TMAZ sides were coarser than the grains found in the as received and annealed metals, as seen in Fig. 8. The effect of the weld process parameters on grain size changes at the advancing side of the thermomechanically affected zone (ATMAZ) and in the retreating side (RTMAZ) was analyzed and the grain measurements are reported in Fig. 8. It is observed that the mean grain diameter at the advancing side is larger than at the retreating side for each rotation speed at the travel speeds of 2.1 and 3.4 mm/s. The smaller-grain measured at the retreating side is most likely caused by the greater-straining expected at this location; two opposite forces act on the material: one is the rotational force imparted by the turning tool as this material is transferred to the back of the tool, and the second is the forward force produced as the tool moves along the plate during friction stir welding. The mean grain

diameter was the same at the lowest travel speed of 1.3 mm/s regardless of the location of the TMAZ or rotation speeds. It was also observed that the effect of travel speed on mean grain size was more significant in the retreating side, where the grain size decreased with the increase of the travel speed (Fig. 8).

3.2 Mechanical Properties of the weld

Tensile tests were conducted of all weld samples, and of base metal samples in the as-received and annealed conditions. The results are presented in Table 2; the as-received base metal sample had the highest strength which corresponds to the finest-grain size of all samples tested, in addition to its partial strain. It was indicated earlier that the annealed sample experienced grain growth compared to the as-received metal, but the grains were still finer than those measured in the friction stir welds, consequently its tensile properties were lower than the as-received metal, but higher than the coupon welds. The best friction stir weld was the one fabricated at 2000 rpm—3.4 mm/s that recorded a tensile strength at 75% of the as-received metal, and yield strength at 51% of the parent metal. The large grain sizes and lower strengths of the welds suggest that dynamic recrystallization and grain growth has taken place. The elongation of the annealed sample (22%) was higher than that of the parent metal (11.0%), while the FSW produced at 2000 rpm—3.4 mm/s was only 2.8%.

All cross-weld tensile samples failed at the advancing side of the weld; it was a 45° shear fracture. The fractured surfaces of the weld tensile specimens were examined and show a lamellar-like failure mode, as shown in Fig. 9. No dispersoids were observed in the fracture surface that could be connected with this prefer failure location. A detailed evaluation of the microstructure of the entire cross-weld displays a sharp heterogeneous microstructure at the stirred zone/TMAZ interface on the advancing side (Fig. 10) that must have influenced the failure at this location. In contrast the retreating side shows a microstructure that is more homogeneous and undergoes a more gradual change, as it is observed in Fig. 11. These resulting microstructures at either side of the welds are influenced by the metal flow characteristics associated with the friction stir welding process. The flow patterns of the plasticized material have been studied by several investigators, Fig. 12 shows the schematic of one of the models that has been developed (Ref 12). It can be reasoned that the material at the advancing side experiences a "straight through current" since the tool rotation is in the same direction as the travel direction and the material just

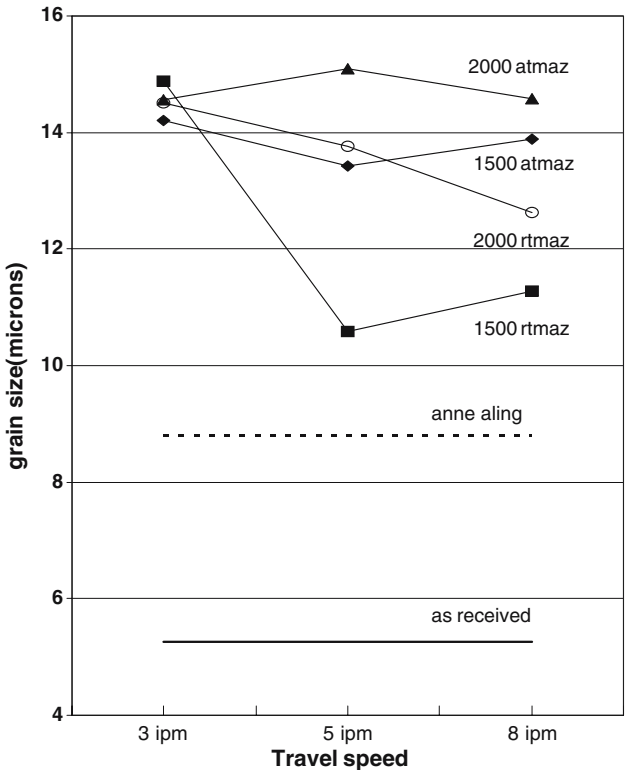

Fig. 8 Grain sizes at both sides of the TMAZ

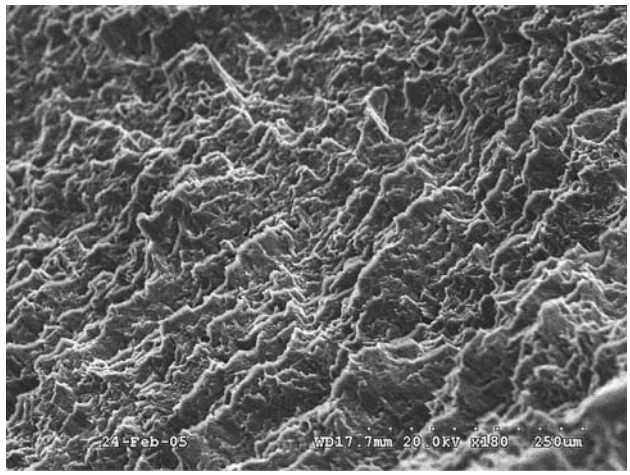

Fig. 9 SEM fractograph of FSW cross-weld tensile sample

Table 2 Mechanical properties of the base metal and welds

Condition	Yield Strength, MPa, psi	% YS of Base Metal	Tensile Strength, MPa, psi	% TS of Base Metal
As received	227.6 (33,007)	100	307.7 (44,631)	100
Annealed	189.4 (27,476)	83.0	263.3 (38,192)	87.0
1500 rpm—1.3 mm/s (3 ipm)	99.1 (14,369)	43.5	209.3 (30,364)	69.6
1500 rpm—2.1 mm/s (5 ipm)	94.9 (13,765)	41.7	200.0 (28,992)	66.4
1500 rpm—3.4 mm/s (8 ipm)	98.5 (14,282)	43.3	205.6 (29,818)	68.3
2000 rpm—1.3 mm/s (3 ipm)	114.7 (16,636)	50.4	216.2 (31,366)	71.9
2000 rpm—2.1 mm/s (5 ipm)	111.0 (16,096)	48.8	220.2 (31,931)	73.3
2000 rpm—3.4 mm/s (8 ipm)	115.3 (16,722)	50.7	225.6 (32,705)	75.0

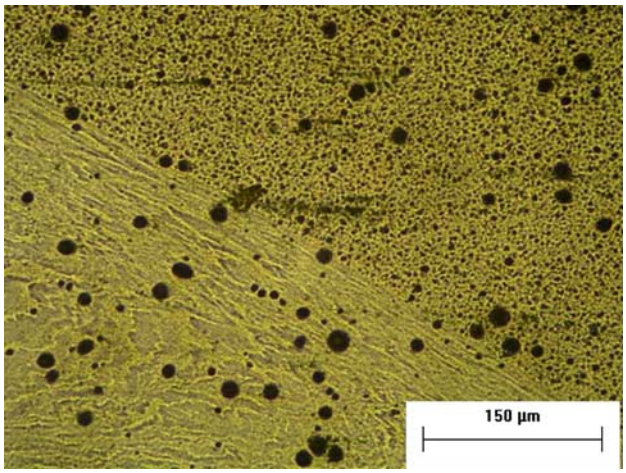

Fig. 10 Micrograph showing the microstructure contrast at the advancing side

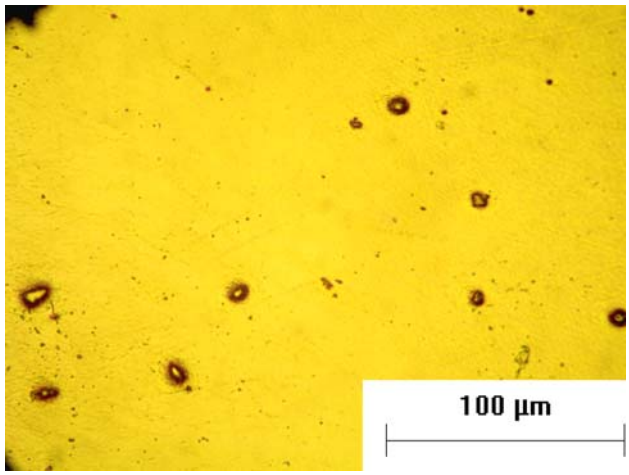

Fig. 11 Micrograph displays a homogeneous microstructure at the retreating side

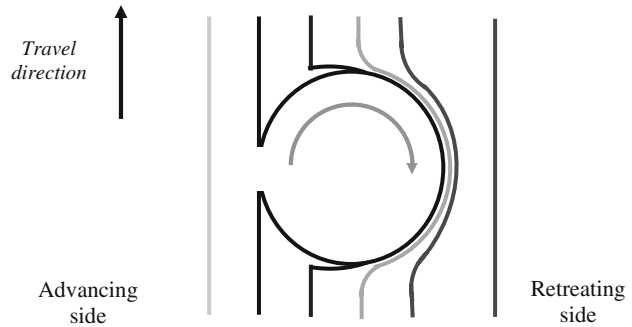

Fig. 12 Streamline metal flow around the pin

appears to have been buttered against the base metal in a relative short time. The material at the retreating side, on the other hand, is said to experience "maelstrom current" (Ref 13) and more turbulent flow conditions since the direction of the tool rotation is opposite to the travel direction.

3.3 Corrosion Tests

Pontentiodynamic tests were performed in a range from – 0.02 V vs. OCP (open circuit potential) up to 0.3 V vs. OCP. The scan rate was 0.2 mV/s. Prior to testing the samples were immersed in corrosive water for 1 h. Figure 13 shows the potentiodynamic scan curves. The shape of the curves suggests uniform anodic dissolution with a pseudo-passivation. Compared to the base metal, the welded samples show a slightly higher OCP. The annealed sample exhibits an OCP between that for the base metal and the welded samples. Table 3 shows the OCP value for all the samples registered before the scan.

The shape of anodic dissolution curve is same for all the samples tested, suggesting that the anodic dissolution mechanism for the FS welds, annealed sample and as-received sample is the same. However, due to the negative difference effect (NDE), the corrosion rates of the samples cannot be measured by the Tafel slopes. There are three reactions occurring on the work piece: anodic dissolution of magnesium, anodic hydrogen evolution, and cathodic hydrogen evolution. The cathodic hydrogen evolution from the noncorroded areas should be different from that of the corroding areas. Hence, the polarization curve may not necessarily follow a simple Tafel equation and the corrosion rate at the corrosion potential cannot be estimated through Tafel extrapolation. The hydrogen evolution increases as the applied polarization potential becomes more positive. It is the characteristic feature of magnesium and its alloys.

The corrosion behavior of the samples was also studied by electrochemical impedance spectroscopy (EIS). The potentiodynamic and EIS data was obtained by exposing the top area of the friction stir weld. Figure 14 shows the Nyquist plots of the weld, annealed, and as-received samples after immersion in the corrosive water for 1 h. The impedance spectra's exhibits three components for all the samples: Two capacitive loops and one inductive loop. This point to the same corrosion mechanism for all the samples tested. Similar loops were observed in electrochemical studies of magnesium and alloy by several researchers (Ref 14-16). The first capacitive loop, at high and intermediate frequencies, has been attributed by all investigators to the charge transfer process. The second capacitive loop, at lower frequencies is attributed to mass transfer process in the oxide and hydroxide layers. Furthermore, an inductive trend attributed to adsorption processes is observed at lower frequencies. The friction stir weld samples fabricated at 1500 rpm—1.3 mm/s and 2000 rpm—3.4 mm/s represent the two extreme cases in terms of the heat input and the strain induced in the material. However, the impedance plots of the two friction stir welds tested seem to overlap indicating that the values of capacitance and inductance are similar. The values of the electrochemical parameters R_{ct} and $1/R_{ct}$ based on a fitted model for the first loop are shown in Table 4. Both parameters are larger in the case of the friction stir welds compared to the annealed and as-received material, suggesting an improvement in the corrosion resistance in case of the welds since $1/R_{ct}$ is directly proportional to the corrosion rate.

In order to compare the data obtained by EIS techniques, all four samples were immersed in the corrosive water for 6 days, at room temperature. The corrosion rates were evaluated in each case and the results are as presented in Table 5. The corrosion rate evaluated by immersion of the as-received material is highest of all the samples tested. This supports the

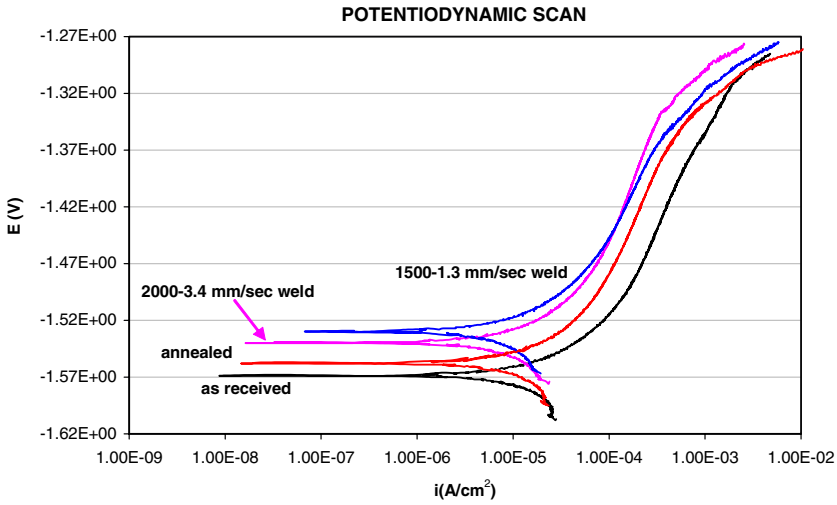

Fig. 13 Potentiodynamic scans of four test samples which includes two friction stir welds, as-received sample and an annealed sample

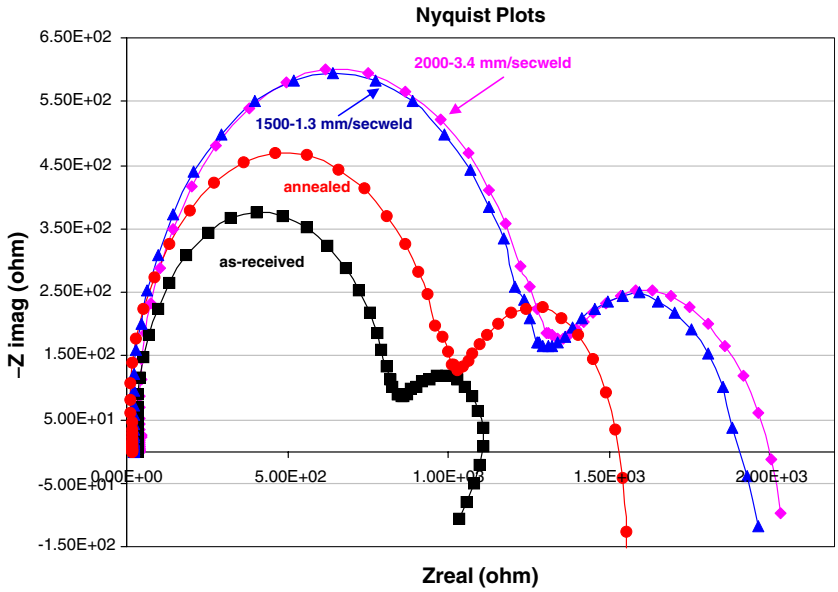

Fig. 14 Nyquist plots comparing the corrosion behavior of four samples: two FS welds, as-received sample, and annealed sample

Table 3 OCP values before the potentiodynamic scan

Sample	OCP (V)
Base metal (as received)	−1.581
Annealed base metal	−1.569
2000 rpm—3.4 mm/s (8 ipm) weld	−1.548
1500 rpm—1.3 mm/s (3 ipm) weld	−1.540

Table 4 Values of electrochemical parameters based on fitted model

Condition	R_{ct}	$1/R_{ct}$
As received	775	0.001290 (1.29×10^{-3})
Annealed	999	0.001001 (1.01×10^{-3})
1500 rpm—1.3 mm/s (3 ipm) weld	1250	0.000800 (0.80×10^{-4})
2000 rpm—3.4 mm/s (8 ipm) weld	1275	0.000784 (0.78×10^{-4})

Table 5 Corrosion rates of immersed samples

Condition	Corrosion rate kpy (mpy)
As received	29.5 (18.34)
Annealed	15.1 (9.39)
1500 rpm—1.3 mm/s (3 ipm) weld	22.8 (14.16)
2000 rpm—3.4 mm/s (8 ipm) weld	21.6 (13.44)

result obtained in EIS measurements in which the as-received material showed the highest value of $1/R_{ct}$.

4. Conclusions

1. Sound friction stir welds were fabricated with the AZ31B-H24 Mg-alloy. The tensile strength of the best

weld was about 75% of the as-received base metal, produced at 2000 rpm rotational tool speed and 3.4 mm/s (8 ipm) travel speed.
2. The grain sizes in the weld nugget and TMAZ were coarser than those found in the as-received base metal and annealed sample. The coarser-grains and the lower-tensile strengths of the friction stir welds suggest that dynamic recrystallization and grain growth may have occurred in these welds.
3. All weld tensile samples failed in the advancing side at the stirred zone/TMAZ interface.
4. Dispersoids segregated to the weld stirred zone/TMAZ interface by advancing side; however no dispersoids were found on the fractured surface of the weld samples. This implies that the failure was most likely the result of the heterogeneous microstructure at this location.
5. Corrosion tests show that the welds had similar corrosion behavior, and showed improved corrosion behavior when compared to the base metal.

References

1. W.M. Thomas, International patent application No. PCT/CB92/02202, GB Patent No. 9125978., 1991, p 8, Dec 6
2. F. Pravdic, H. Kaufmann, Vertical Chill Casting of Magnesium Alloy. Light metals age., 2003, p 28–31, October 2003
3. Magnesium and magnesium alloy, ASM Specialty Handbook, ASM International, 1999, p 194–199
4. B.L. Mordike and T. Ebert, Magnesium – Properties, Applications, Potential, *Mater. Sci. Eng. A*, 2001, **302**, p 37–45
5. J.H. Ouyang, D. Jandric, R. Kovacevic, M. Song, M. Valant, Visualization of Material Flow During Friction Stir Welding (FSW) of the Same and Dissimilar Aluminum Alloys, Trends in Welding Research, 15-19 April 2002, Pine Mountain, Georgia, ASM International, p 229–234
6. Magnesium and magnesium alloy, ASM Specialty Handbook, ASM International, 1999, p 274
7. J.C. Tan and M.J. Tan, Dynamic Continuous Recrystallization Characteristics in Two Stage Deformation of Mg-3Al-1Zn Alloy Sheet, *Mater. Sci. Eng. A*, 2003, **339**, p 124–132
8. J.A. Esparaza, W.C. Davis, and L.E. Murr, Friction-Stir Welding of Magnesium Alloy AZ31B, *J. Mater. Sci. Lett.*, 2002, **21**, p 17–20
9. C. Zener and H.H. Hollomon, Effect of Strain Rate Upon Plastic Flow of Steel, *J. Appl. Phys.*, 1944, **15**, p 22–32
10. C.I. Chang, C.J. Lee, and J.C. Huang, Relationship between Grain Size and Zener–Hollomon Parameter During Friction Stir Processing in AZ31 Mg Alloys, *Scripta Materialia*, 2004, **51**, p 509–514
11. Barnett M.R. Effect of Grain Size on the Deformation and Dynamic Recrystallization of Mg-3Al-Zn, Materials Science Forum 467–470, 2004, p 435–440
12. T.U. Seidel, Two-Dimensional Friction Stir Welding Process Model Based on Fluid Mechanics, *Reynolds AP Sci. Technol. Welding Joining*, 2003, **8**(3), p 175–183
13. J.A. Schneider and A.C. Nunez, Characterization of Plastic Flow and Resulting Microtextures in Friction Stir Weld, *Metallurg. Mater. Trans. B*, 2004, **35**, p 777
14. G. Song, A. Atrens, D. John, X. Wu, and J. Nairn, The Anodic Dissolution of Magnesium in Chloride and Sulphate Solutions, *Corr. Sci.*, 1997, **39**, p 1981–2004
15. G. Baril and N. Pebere, The Corrosion of Pure Magnesium in Aerated and Deaerated Sodium Suplhate Solutions, *Corr. Sci.*, 2001, **43**, p 471–484
16. L. Kouisini, M. Azzi, F. Dalard, and S. Maximovitch, Phosphate Coatings on Magnesium Alloy AM60 Part 2: Electrochemical Behavior in Borate Buffer Solution, *Surf. Coatings Technol.*, 2005, **192**, p 239–246